Engineering Science and Technology, an International Journal xxx (2016) xxx–xxx

HOSTED BY
ELSEVIER

Contents lists available at ScienceDirect

Engineering Science and Technology, an International Journal

journal homepage: www.elsevier.com/locate/jestch

Full Length Article

Mass transfer and power characteristics of stirred tank with Rushton and curved blade impeller

Thiyam Tamphasana Devi [a], Bimlesh Kumar [b,*]

[a] Civil Engineering, NIT Manipur, India
[b] Civil Engineering, IIT Guwahati, Guwahati 781039, India

ARTICLE INFO

Article history:
Received 21 July 2016
Revised 21 October 2016
Accepted 7 November 2016
Available online xxxx

Keywords:
Curved blade impeller
CFD
Gas-liquid
Mass transfer coefficient
Power draw

ABSTRACT

Present work compares the mass transfer coefficient (k_La) and power draw capability of stirred tank employed with Rushton and curved blade impeller using computational fluid dynamics (CFD) techniques in single and double impeller cases. Comparative analysis for different boundary conditions and mass transfer model has been done to assess their suitability. The predicted local k_La has been found higher in curved blade impeller than the Rushton impeller, whereas stirred tank with double impeller does not show variation due to low superficial gas velocity. The global k_La predicted has been found higher in curved blade impeller than the Rushton impeller in double and single cases. Curved blade impeller also exhibits higher power draw capability than the Rushton impeller. Overall, stirred tank with curved blade impeller gives higher efficiency in both single and double cases than the Rushton turbine

1. Introduction

Gas-liquid tanks are widely used in several process industries to carry out various gas-liquid reactions [36,14]. The characteristic of fluid dynamics in such tanks is generally understood through the mechanism of interaction between the two phases (gas-liquid) in terms of mass transfer. Studies based on gas-liquid phase in stirred tank were done by several researchers [17,1,30] to predict the mass transfer coefficient in stirred tank. Mass transfer depends on various factors like types and number of impeller, gas superficial velocity and impeller speed. Researchers have used different models to predict mass transfer coefficient such as Higbie Penetration model [13] and surface renewal model [6]. Gimbun et al. [12] used Higbie and Danckwerts model to predict mass transfer on single impeller of Rushton and curved blade impeller. Ranganathan and Sivaraman [30] used two more models apart from above mentioned which are based on slip velocity (difference of gas velocity and liquid velocity).

One of the other significant design parameters for a multiphase stirred tank reactor is the power draw by the agitator which is affected by the physical properties, operating parameters, and geometrical parameters. It is defined as the amount of energy necessary in a period of time, in order to generate the movement of the fluid within a vessel by means of mechanical or pneumatic agitation [32]. Economic selection criteria for an impeller are greatly influenced by the power input for stirred tank application. Researchers [24,23,32] have proposed different correlations to quantify the gassed power input (gas-liquid phase) since the power input is significantly different from gas-liquid phase (gassed condition) and liquid–liquid phase (ungassed condition).

Impeller types and number plays vital role in mass transfer and power consumptions in gas-liquid stirred tanks. Study of Rushton impeller [16,38,21,1] for mass transfer and power input is widely available in literature, however, study forcurved blade impeller is found very less in literarure except few studies done by Myers et al. [27]; Gimbun et al. [12] and Devi and Kumar [7]. In this study, Rushton and curved blade impeller in single and double case is being studied in gas-liquid phase taking constant bubble diameter with Eulerian-Eulerian multiphase model. This study aims in predicting mass transfer and power draw and comparing with published literature.

2. Numerical model

Eulerian-Eulerian multiphase model is used to simulate the hydrodynamics of flow in this study. The continuous and disperse phases are treated as interpenetrating media identified by their local volume fractions. The Reynolds averaged mass and momentum balance equations are solved for each of the phases and are given as follows:

* Corresponding author.
E-mail address: bimk@iitg.ernet.in (B. Kumar).
Peer review under responsibility of Karabuk University.

http://dx.doi.org/10.1016/j.jestch.2016.11.005
2215-0986/© 2016 Karabuk University. Publishing services by Elsevier B.V.

Please cite this article in press as: T.T. Devi, B. Kumar, Mass transfer and power characteristics of stirred tank with Rushton and curved blade impeller, Eng. Sci. Tech., Int. J. (2016), http://dx.doi.org/10.1016/j.jestch.2016.11.005

Nomenclature

a	interfacial area [L^{-1}]	P_g	gassed power input [ML^{-1}]
C_μ, $C_{1\varepsilon}$, $C_{2\varepsilon}$, $C_{3\varepsilon}$, σ_k, σ_ε	constants [–]	Q_g	flow rate [$L^3\,T^{-1}$]
C_D	drag coefficient [–]	$\vec{R}_i$	inter-phase forces [$ML\,T^{-2}$]
c	constant [–]	Re	Reynolds number [–]
$C_{kL}a$, a, b	constants [–]	Re_p	relative Reynolds number [–]
d	impeller diameter [L]	s	surface renewal rate [T^{-1}]
d_b	bubble diameter [L]	Δt	impeller thickness [L]
D_l	liquid diffusion coefficient [$L^2\,T^{-1}$]	t	time [T]
$\vec{F}_i$	Coriolis and centrifugal forces [$ML\,T^{-2}$]	T	tank diameter [L]
Fl_g	flow number [–]	t_e	contact time [–]
F_r	Froude number [–]	$\vec{U}_i$	mean velocity of ith phase [$L\,T^{-1}$]
$\vec{g}$	acceleration due to gravity [$L\,T^{-2}$]	u_{slip}	slip velocity [$L\,T^{-1}$]
G_{kl}	rate of production of turbulent kinetic energy [$ML^{-1}\,T^{-2}$]	V	volume of tank [L^3]
$\bar{\bar{I}}$	unit tensor [–]	v_g	superficial gas velocity [$L\,T^{-1}$]
k_i	turbulent kinetic energy of ith phase [$L^2\,T^{-2}$]	v_l	kinematic liquid viscosity [$L^2\,T^{-1}$]
K	constant in Eq. 14 [–]	w	width of blade [L]
K	exchange coefficient [$ML^{-3}\,T^{-1}$]	α_i	volume fraction of ith phase [–]
k_L	mass transfer coefficient [$L\,T^{-1}$]	$\bar{\bar{\tau}}_{eff}$	effective stresses [$ML^{-1}\,T^{-2}$]
k_La	volumetric mass transfer coefficient [T^{-1}]	$\bar{\bar{\tau}}_{lam}$	laminar stress [$ML^{-1}\,T^{-2}$]
$\langle k_La\rangle$	average mass transfer coefficient [T^{-1}]	$\bar{\bar{\tau}}_t$	turbulent stress [$ML^{-1}\,T^{-2}$]
N	impeller speed [T^{-1}]	ρ_i	density of ith phase [$M\,L^{-3}$]
N_{p0}	single phase power number [–]	ε	dissipation rate [$L^2\,T^{-3}$]
p	pressure [$ML^{-1}\,T^{-2}$]	μ_l	liquid viscosity [$ML^{-1}\,T^{-1}$]
P_g/P_0	relative power draw [–]	π	3.14 [–]
		τ	torque [$ML^2\,T^{-2}$]

Continuity equation:

$$\frac{\partial}{\partial t}(\alpha_i\rho_i) + \nabla.(\alpha_i\rho_i\vec{U}_i) = 0 \tag{1}$$

$$\alpha_l + \alpha_g = 1 \tag{2}$$

where, ρ_i, α_i and $\vec{U}_i$ are density, volume fraction and mean velocity, respectively, of phase i (l or g).

Momentum equation:

$$\frac{\partial}{\partial t}(\alpha_i\rho_i\vec{U}_i) + \nabla\cdot(\alpha_i\rho_i\vec{U}_i\vec{U}_i) = -\alpha_i\nabla p + \nabla\bar{\bar{\tau}}_{\mathrm{effi}} + \vec{R}_i + \vec{F}_i + \alpha_i\rho_i\vec{g} \tag{3}$$

where, p is the pressure shared by the two phases and $\vec{R}_i$ is the inter-phase momentum exchange terms. $\vec{F}_i$, represents the Coriolis and centrifugal forces applies in MRF (multiple reference frame) impeller model which is used in this study as impeller model. The Reynolds stress tensor $\bar{\bar{\tau}}_{\mathrm{effi}}$ is the laminar and turbulent stresses and by Boussinesq hypothesis, it is given as

$$\bar{\bar{\tau}}_{\mathrm{effi}} = \alpha_i(\mu_{\mathrm{lam},i} + \mu_{t,i})(\nabla\vec{U}_i + \nabla\vec{U}_i) - \frac{2}{3}\alpha_i(\rho_ik_i + (\mu_{\mathrm{lam},i} + \mu_{t,i})\nabla.\vec{U}_i\Big)\bar{\bar{I}} \tag{4}$$

$\mu_{\mathrm{lam},i}$ and $\mu_{t,i}$ are laminar and turbulent viscosity. k_i is turbulent kinetic energy and $\bar{\bar{I}}$ is unit tensor.

2.1. Turbulence model

Standard k-ε turbulence model [29] with dispersed k-ε multiphase turbulence model is used in this study to simulate the gas-liquid phase flow as gas is dispersed in continuous liquid. The governing equations of turbulent kinetic energy, k and turbulent dissipation rate, ε, are solved only for liquid phase as:

$$\frac{\partial}{\partial t}(\rho_l\alpha_lk_l) + \nabla.(\rho_l\alpha_l\vec{U}_lk_l) = \nabla\cdot\left(\alpha_l\frac{\mu_{t.l}}{\sigma_k}\nabla k_l\right) + \alpha_lG_{kl} - \rho_l\alpha_l\varepsilon_l + \rho_l\alpha_l\prod_{kl} \tag{5}$$

$$\frac{\partial}{\partial t}(\rho_l\alpha_l\varepsilon_l) + \nabla\cdot\left(\rho_l\alpha_l\vec{U}_l\varepsilon_l\right) = \nabla.(\alpha_l\frac{\mu_{t.l}}{\sigma_\varepsilon}\nabla\varepsilon_l) + \alpha_l\frac{\varepsilon_l}{k_l}(C_{1\varepsilon}G_{kl} - C_{2\varepsilon}\rho_l\varepsilon_l) + \rho_l\alpha_l\prod_{\varepsilon l} \tag{6}$$

Turbulent liquid viscosity is given as:

$$\mu_{t.l} = \rho_lC_\mu\frac{k_l^2}{\varepsilon_l} \tag{7}$$

G_{kl} is the rate of production of turbulent kinetic energy. $\prod_{kl}$ and $\prod_{\varepsilon l}$ represents the influence of the dispersed phase on the continuous phase [8]. C_μ, $C_{1\varepsilon}$, $C_{2\varepsilon}$, $C_{3\varepsilon}$, σ_k and σ_ε are constants of standard k-ε model. Their values are 0.09, 1.44, 1.92, 1.2, 1.0 and 1.3 respectively.

2.2. Inter-phase momentum exchange

Only drag force is considered in the present work as other forces (lift and virtual) have been neglected because of its less significance in phase interaction [18]. Hence, $\vec{R}_i$ from Eq. (3) reduced only to drag force as:

$$\vec{R}_l = -\vec{R}_g = K(\vec{U}_g - \vec{U}_l) \tag{8}$$

K is the liquid-gas exchange coefficient given as:

$$K = \frac{3}{4}\rho_l\alpha_l\alpha_g\frac{C_D}{d_b}|\vec{U}_g - \overleftarrow{U}_l| \tag{9}$$

d_b is the bubble diameter and C_D is the drag coefficient defined as function of relative Reynolds number, Re_p. The standard formulation of Re_p does not account the effect of turbulence on bubble movement. Hence Re_p has been modified to include the effect of turbulence [17]:

$$Re_p = \frac{\rho_l|\vec{U}_g - \vec{U}_l|d_b}{\mu_l + C\mu_{T,l}} \tag{10}$$

C is the model parameter introduced to account for the effect of the turbulence in reducing slip velocity. This parameter is set to 0.3 [17]. Drag coefficient is then calculated using standard correlation of Schiller and Naumann which is written as:

$$C_D = \begin{cases} \frac{24\left(1+0.15\ Re_p^{0.687}\right)}{Re_p}, & Re_p \leqslant 1000 \\ 0.44, & Re_p > 1000 \end{cases} \tag{11}$$

2.3. Mass transfer model

There are several models available in literature for calculating local mass transfer co-efficient (k_L) but commonly used model are based on penetration theory and surface renewal model when the bubble diameter is known. By Higbie [13] penetration theory, the liquid phase mass transfer coefficient of a bubble with a mobile surface is represented as

$$k_L = \frac{2}{\sqrt{\pi}}\sqrt{\frac{D_l}{t_e}} \tag{12}$$

where t_e is the contact time and is calculated based on Kolmogorov's Length scale of isotropic turbulence as $t_e = \sqrt{v_l/\varepsilon_l}$; ε_l is turbulent dissipation rate and v_l is the kinematic viscosity of liquid. So, Eq. (12) becomes as

$$k_L^{penetration} = \frac{2}{\sqrt{\pi}} D_l^{0.5}\left(\frac{\varepsilon_l}{v_l}\right)^{0.25} \tag{13}$$

And this model is denoted as $k_L^{penetration}$. Refinement of the penetration theory, mass transfer co-efficient, k_L, suggested by Danckwerts [6] is given as $k_L = \sqrt{D_l s}$, where s is the surface renewal rate. This approach assumed that k_L is related to the average surface renewal rate resulting from exposure of the bubble interface to the turbulent eddies with a variable contact time. Later, Lamont and Scott [22] assumed that the small-scale turbulent motion, which extends from smallest viscous motion to inertial ones, affects the rate of mass transfer and s is calculated based on Komogorov's theory of isotropic turbulence. Hence, Eq. (12) becomes as

$$k_L^{eddy\ cell} = K\ D_l^{0.5}\left(\frac{\varepsilon_l}{v_l}\right)^{0.25} \tag{14}$$

where, D_l is the diffusion co-efficient and ε_l is the turbulent dissipation rate in the liquid phase; v_l is the liquid dynamic viscosity and $K = 0.4$ is model constants. This model is denoted as $k^{eddy\ cell}$ and generally referred as eddy cell model. Caderbank [5] further assumed that the bubble is having a mobile interface and gross mean flow of liquid relative to the bubble (slip velocity) controls the renewal of liquid phase and contact time can be expressed in terms of average bubble size and average slip velocity as

$$k_L^{slip\ velocity} = \frac{2}{\sqrt{\pi}}\sqrt{\frac{D_l u_{slip}}{d_b}} \tag{15}$$

u_{slip} can be obtained from phase velocity difference from an Eulerian-Eulerian two-fluid CFD simulation. And the expression of this model is denoted as $k_L^{slip\ velocity}$. Alves et al. [2] modified the equation of k_L based on bubble rigidity and is denoted as k_L^{rigid}. And this is obtained from the equation proposed by Frossling [10] based on laminar boundary value theory as

$$k_L^{rigid} = c\left(\frac{u_{slip}}{d_b}\right)^{0.5} D_l^{2/3} v_l^{-1/6} \tag{16}$$

where, c is a constant of value 0.6. And volumetric mass transfer co-efficient ($k_L a$) is the combination of k_L and a, where a is the interfacial specific area and is a function of local volume fraction, α_g and bubble diameter, d_b. Therefore, a is expressed as

$$a = \frac{6\alpha_g}{d_b} \tag{17}$$

2.4. Power draw

The power delivered to the fluid is the product of the impeller speed, $2\pi N$ and torque, τ. And it is a crucial characteristic of stirred tank reactors [37]. The prediction of gassed power input, P_g was calculated from the moment acting on the shaft and impeller. The calculated torque is related with gassed power input as:

$$P_g = 2\pi N\tau \tag{18}$$

Ungassed power number, N_{p0} is generally expressed in terms of ungassed power input, P_0 and is given as below for single Rushton impeller [4].

$$N_{p0} = \frac{P_0}{\rho_l N^3 d^5} = 2.512\left(\frac{\Delta t}{d}\right)^{-0.195} T^{0.063} \tag{19}$$

where ρ_l, N and d are the density of liquid, impeller speed and impeller diameter respectively. Δt and T are the impeller thickness and tank diameter. Smith [31] proposed the relative power draw, P_g/P_0, from the measurements of Warmoeskerken and Smith [35] and Gezork et al. [11] for single Rushton impeller as below:

$$\frac{P_g}{P_o} = 0.18 Fr^{-0.2} Fl_g^{-0.25} \tag{20}$$

F_r is the Froude number and is calculated as $\frac{N^2 d}{g}$; g is the gravitational force. Fl_g is flow number and is calculated as $\frac{Q_g}{ND^3}$; Q_g is flow rate. Taghavi et al. [32] suggested a correlation for P_0 from experimental observation for dual impellers as:

$$\frac{P_o}{V} = 6\times 10^{-12} Re^{2.921}, \qquad Re > 10^4 \tag{21}$$

They further proposed a correlation of P_g/P_0, based on the experimental and simulation results of dual Rushton impeller as:

$$\frac{P_g}{P_o} = 0.19(Fl_g)^{-0.28}(Fr)^{0.127}\left(\frac{w}{d}\right)^{0.18}\left(\frac{d}{T}\right)^{-0.65} \tag{22}$$

The above correlations of P_g/P_0 are based on Rushton impeller for single (from Eq. (19) to Eq. (20)) and for double (Eq. (21) and (22)). However, for other impeller types like curved blade impeller which is used in this study, the following correlation originally proposed by Hugmark [15] for six blade Rushton impeller is used in this study and this correlation is reapplied by Moucha et al. [25] for other impellers as:

$$\frac{P_g}{P_o} = 0.1\left(\frac{N^2 d^4}{gwV^{2/3}}\right)^{-0.2}\left(\frac{Q_g}{NV}\right)^{-0.25} \tag{23}$$

where w and V are the width of blade and tank volume respectively. The energy per unit mass available in a stirred tank which can be applied in different types of impeller is given as:

$$\varepsilon = \frac{P_g}{\rho_l V} \Rightarrow P_g = \varepsilon\rho_l V \tag{24}$$

So, for other types of impeller Eq. (24) is used to P_g as ε varies for different types of impeller and substituting the value of P_g in Eq. (23) to get P_0 as:

$$P_0 = \frac{\rho_l V\varepsilon}{\left[0.1\left(\frac{N^2 d^4}{gwV^{2/3}}\right)^{-0.2}\left(\frac{Q_g}{NV}\right)^{-0.25}\right]} \tag{25a}$$

Then using the simulated CFD value of P_g from Eq. (18), final correlation P_g/P_0 is calculated for different types of impeller as:

$$\frac{P_g}{P_0} = \frac{2\pi N\tau\left[0.1\left(\frac{N^2d^4}{gwV^{2/3}}\right)^{-0.2}\left(\frac{Q_g}{NV}\right)^{-0.25}\right]}{\rho_l V\varepsilon} \tag{25b}$$

In this study, Eq. (25b) is used for single and double impeller of both Rushton and curved blade impeller for comparing P_g/P_0 with other correlations. The global mass transfer co-efficient $\langle k_L a\rangle$ for an air-water stirred tank is given as:

$$\langle k_L a\rangle = C_{k_L a}\left(\frac{P_g}{V}\right)^a v_g^b \tag{26}$$

According to Van't Riet [33], the values of constant $C_{kL}a$, a and b are 0.026, 0.4 and 0.5 respectively obtained from a fit to experimental measurements.

3. Solution domain and boundary conditions

Table 1 shows different geometrical dimensions with different boundary conditions. Water is filled up to the height of T and $2T$

Table 1
Geometrical configurations of Rushton and curved blade impeller.

Case	T (m)	d (m)	N (rpm)	v_g (m/s)	d_b (mm)	Boundary condition at top surface	Impeller Types	Impeller No.
1	0.63	0.21	390	0.0074	5.3	Velocity-inlet	Rushton	1
2	0.63	0.21	390	0.0074	5.3	Degassing	Rushton	1
3	0.63	0.21	390	0.0074	5.3	Velocity-inlet	curved blade	1
4	0.63	0.21	390	0.0074	5.3	Degassing	curved blade	1
5	0.26	0.086	698	0.003	3.4	Degassing	curved blade	1
6	0.292	0.0973	450	0.0025	2	Symmetry	Rushton	2
7	0.292	0.0973	450	0.0025	2	Degassing	Rushton	2
8	0.292	0.0973	450	0.0025	2	Degassing	curved blade	2

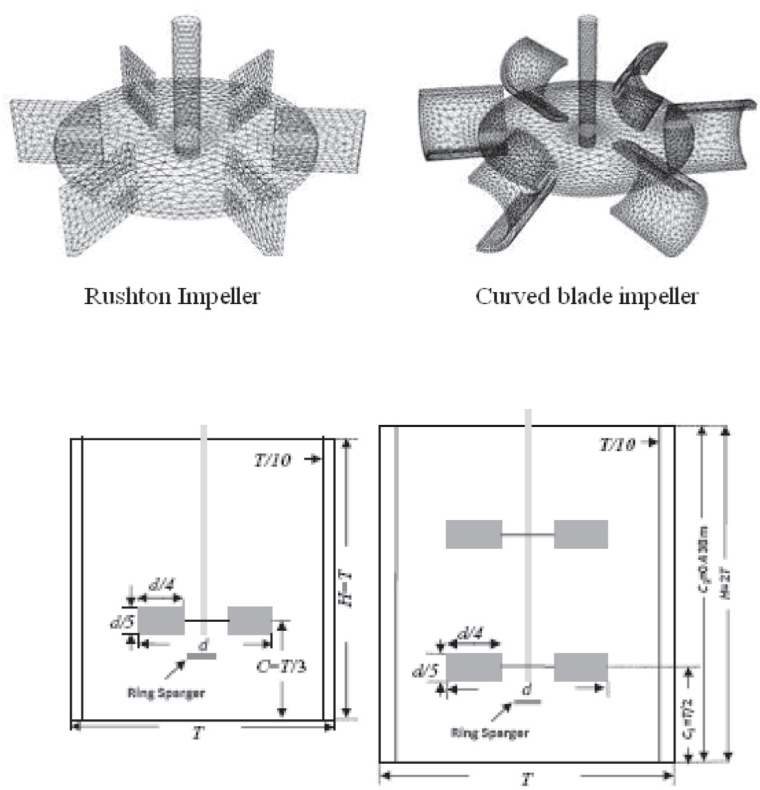

Single Impeller	Double Impeller
$d=T/3$	$d=T/3$
$H=T$	$H=2T$
$C=T/3$	$C_1=T/2$
$b=T/12$	$C_2=(3/2\ T)$
$w=T/2$	$b=T/12$
$t=T/10$	$w=T/2$
	$t=T/10$

Fig. 1. Types of impeller and schemaic diagramm of the stirred tank used in this study.

Please cite this article in press as: T.T. Devi, B. Kumar, Mass transfer and power characteristics of stirred tank with Rushton and curved blade impeller, Eng. Sci. Tech., Int. J. (2016), http://dx.doi.org/10.1016/j.jestch.2016.11.005

for single and double impeller case. Gas is supplied to the liquid through ring sparger which is kept below the impeller. Gas volume fraction of 1 is provided at sparger inlet. Unstructured grids of around 270–520 k cells were generated for single and double impeller stirred tank respectively. Finer grid is employed near the impeller region so that the strong turbulence of fluid flow can be addressed accurately. First order differencing discretization scheme is used to solve the equations of flow, volume fraction and turbulence. Solution is considered as converged when the volume fraction has no significant changes after certain iterations and is achieved when residuals fell nearly below 10^{-4}. Fig. 1 shows the types of impeller used in this study.

Boundary condition plays a crucial role in numerical simulation especially in case where more than one phase is included. Velocity inlet has been assumed at ring sparger [28]. The top surface, which is open to atmosphere, the boundary conditions should satisfy that the gas should escape from the computational domain and liquid is not allowed to escape. Researchers have used various boundary conditions such as walls [34]; velocity-inlet [12,32] and pressure-outlet [19,9]; pressure-inlet and degassing condition [20,26] which is achieved through user defined functions (UDF).

4. Result and discussion

Mass transfer coefficient and power draw will be presented in this section.

4.1. Prediction of mass transfer coefficient (k_La)

Global $\langle k_La \rangle$ is being predicted by using criteria given by on Van't Riet [33]. The comparison of predicted average k_L for different model with literature result is given in Table 2. Penetration and slip velocity model predicts higher k_L values than the other two methods in all cases. Eddy cell model and slip velocity models are fair agreement with the experimental and simulated results of literature and these two models can be considered as the acceptable model for the estimation of k_L. Penetration and eddy cell model does not give the significant difference of k_L for single and double

Table 2
Prediction of k_L and comparison with results of Ranganathan and Sivaraman [25] (bold).

Case	$k_L \times 10^{-3}$ (ms^{-1})				
	CFD				Experimental [2]
	Penetration	Eddy Cell	Slip velocity	Rigid	
1	1.574	0.558	1.138	0.216	
2	1.574	0.558	1.132	0.214	
3	1.528	0.542	0.828	0.157	
4	1.552	0.55	0.730	0.138	
5	1.196	0.424	1.578	0.299	
6	1.616	0.573	1.148	0.218	
7	1.574	0.558	2.411	0.457	0.319
	0.968	0.341	0.275	0.052	
8	1.552	0.55	2.138	0.405	

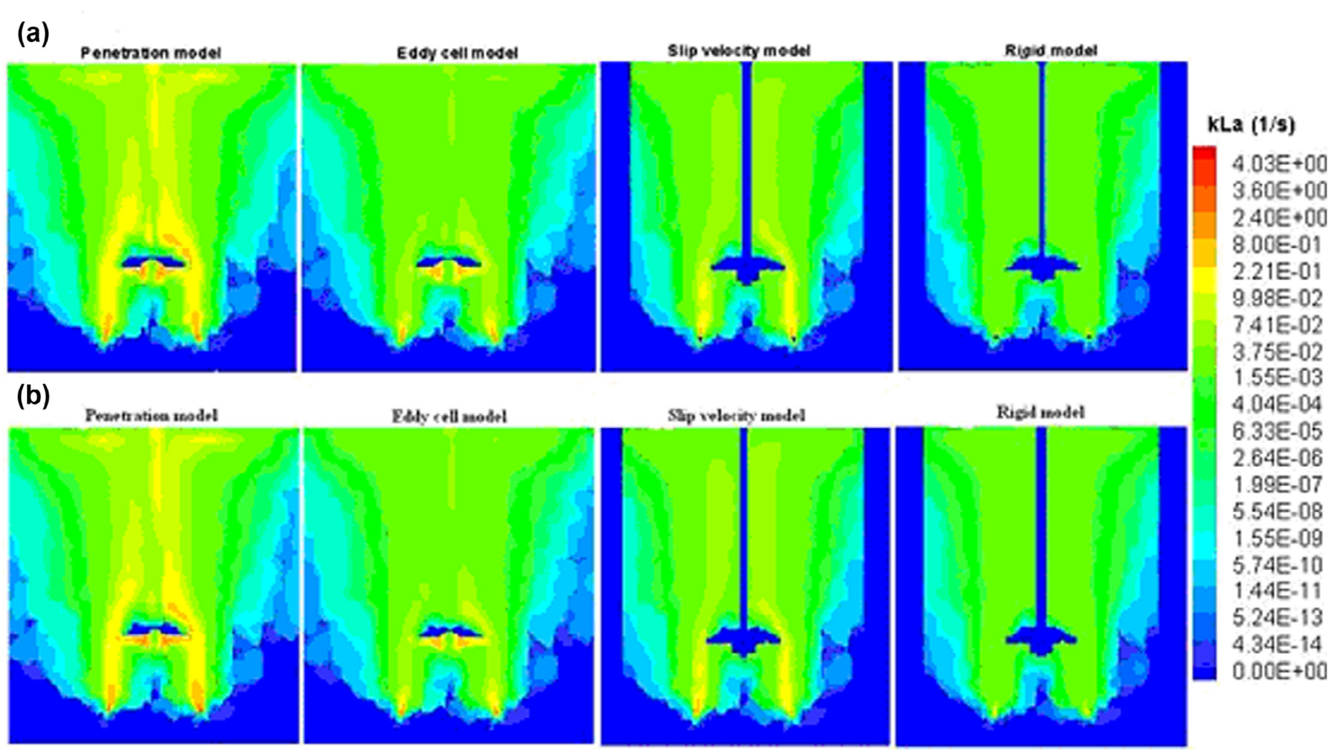

Fig. 2. Distribution of k_La for single (a) Rushton (case 2) and (b) Curved blade impeller (case 4).

Please cite this article in press as: T.T. Devi, B. Kumar, Mass transfer and power characteristics of stirred tank with Rushton and curved blade impeller, Eng. Sci. Tech., Int. J. (2016), http://dx.doi.org/10.1016/j.jestch.2016.11.005

in case of Rushton and curved blade impeller. Variation of k_L is predicted in different boundary conditions.The analysis of local distribution k_La is more important for understanding the phase interaction process in gas-liquid stirred tank efficiency than the global $\langle k_La \rangle$ especially in case when more than one impeller is used. The comparison of distribution of k_La for different models for double Rushton and curved blade impeller is shown in Figs. 3a and 3b.

The prediction of local k_La by penetration model is observed higher than other models (Figs. 2 and 3). Predicted k_La by penetration and eddy cell models are based on dissipation rate and k_La by these two models were observed distributing throughout the tank while in case of slip velocity and rigid model which are based on velocity of gas and water were observed with obstruction by the baffles near the tank wall. The formation of negative pressure zone is observed just above the impeller (upper impeller in case of double impeller). The lower impeller does not form such negative pressure zone (dead zone) because of the influence of the flow circulation generated by the upper impeller (Figs. 3a and 3b). The magnitude of local kLa is found slightly higher (around 5%) in case of double Rushton impeller than the curved blade impeller and this finding is in agreement with Gimbun et al. [12,39]. However, Gimbun et al. [12] argued that this lower value of k_La in curved blade is attributed to several factors and the efficiency of stirred tank was characterized with energy efficiency based on relative power draw rather than k_La which is based on too many processes of interfacial fluid particles. The predicted local k_La is found higher (around 6%) in curved blade impeller than the Rushton impeller in single

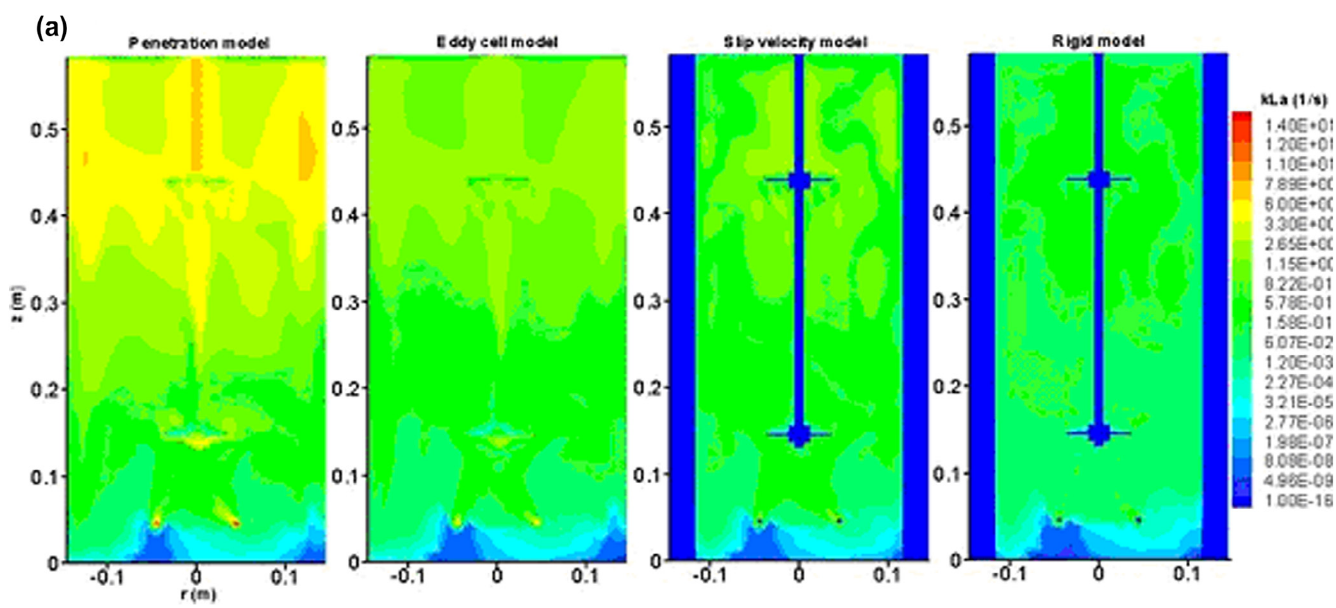

Fig. 3a. Distribution of k_La for double Rushton impeller (case 7).

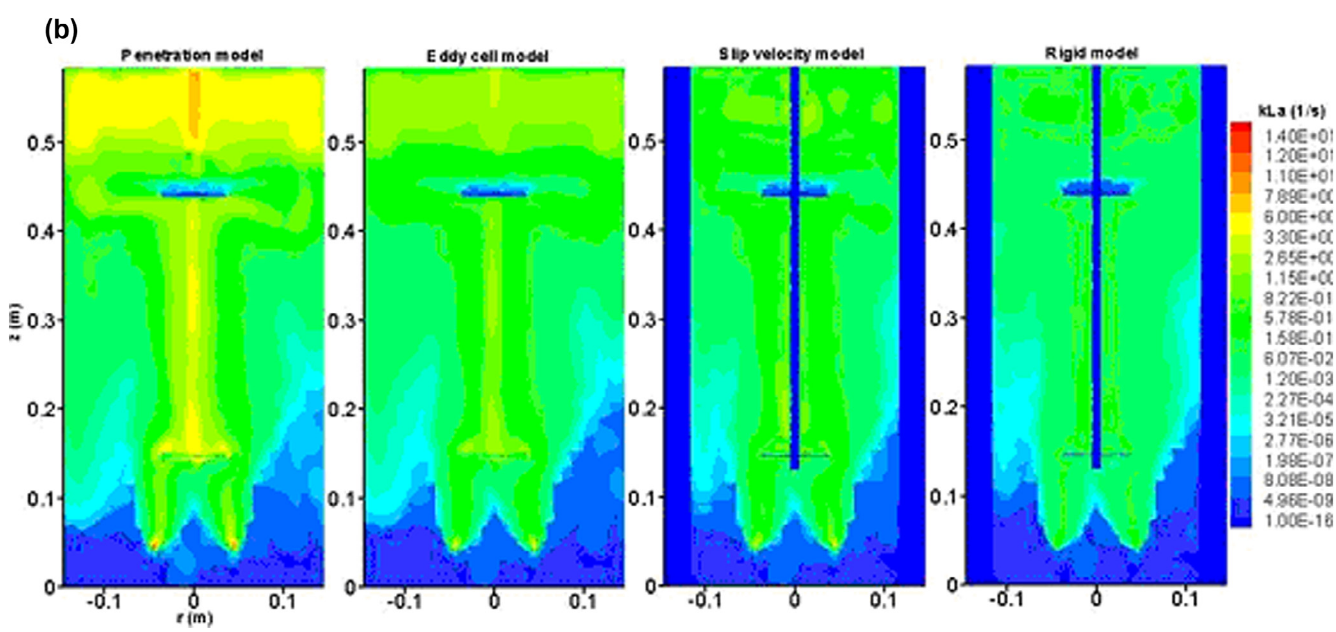

Fig. 3b. Distribution of k_La for double Curved blade impeller (case 8).

Please cite this article in press as: T.T. Devi, B. Kumar, Mass transfer and power characteristics of stirred tank with Rushton and curved blade impeller, Eng. Sci. Tech., Int. J. (2016), http://dx.doi.org/10.1016/j.jestch.2016.11.005

impeller stirred tank. The Bakker's [3] study shows that predicted k_La is same for both multiple Rushton and curved blade impeller in the superficial gas velocity for up to 0.01 m/s and significantly increases the predicted k_La by curved blade impeller beyond this limit. In this study, the superficial gas velocity is within 0.01 m/s (0.0024–0.0074 m/s) and, hence, no such significant difference is predicted between double stirred tank with Rushton and curved blade impeller. The global volumetric k_La predicted based on Eq. (26) is shown in Table 3. The predicted k_La is appeared higher in curved blade than the Rushton impeller in double (15.21%) and in single (6.09%) impeller stirred tank.

4.2. Prediction of power draw

The power draw of gassed condition with respect to the ungassed condition is of important factor to be analyzed for understanding the power draw characteristic in gassed condition. Here, relative power draw (ratio of gassed power input to ungassed power input) is generally introduced to analyze the efficiency. The predicted P_g/P_0 is shown in Table 4 for different cases. Curved blade predicts higher power draw as compared with Rushton impeller. Double impeller also gives higher power draw than the single impeller. The predicted results are in good agreement with published literature. P_g/P_0 is also affected by the imposing boundary condition such as the velocity-inlet boundary condition over-predicts P_g/P_0 than the degassing boundary condition.

The capability of power draw with reference to the single Rushton is shown in Fig. 4. Higher power draw capability is predicted by curved blade (34% in double and 16 % in single case) than the Rushton impeller. Double impeller predicts higher power draw capability (70–80 %) than the single impeller. Correlation of P_g/P_0 applicable for different types of impeller estimates in good agreement with other correlation and with predicted results.

Efficiency of a stirred tank in gas-liquid system can be expressed in terms of energy efficiency and is the qualitative function of power draw and mass transfer rate in the system (Energy = power draw/mass transfer rate). Power draw is taken as the relative power draw; and mass transfer rate as global k_La achieved from Eq. (26) in Table 3. Energy is expressed as efficiency number which is shown in Table 5 for different cases of stirred tank. So, at

Table 3
Prediction of $\langle k_La \rangle$.

Case	P_g/V (watt/m^3)	Van't Riet Eq. (26) $\langle k_La \rangle$ (1/s)	% efficient $\langle k_La \rangle$ of Curved blade over Rushton impeller
1	2706.12	0.0528	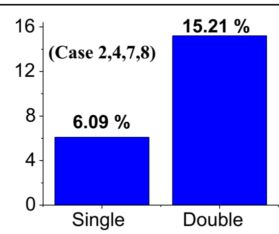
2	1224.34	0.0384	
3	2126.38	0.0479	
4	1432.65	0.0409	
5	707.57	0.0197	
6	789.25	0.0187	
7	1372.69	0.0234	
8	2073.74	0.0276	

Table 5
Overall efficiency of Curved blade over Rushton impeller.

Case	Efficiency number	% overall efficiency of Curved blade over the Rushton impeller
1	18.18	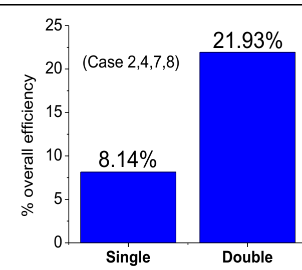
2	11.29	
3	15.73	
4	12.29	
5	41.12	
6	48.05	
7	66.98	
8	85.79	

Table 4
Predictions of P_g/P_0.

	Cases							
	1	2	3	4	5	6	7	8
Present work	0.96	0.43	0.75	0.51	0.81	0.9	1.56	2.37
Gimbun et al. [12]		0.38			0.75			
Myers et al. [27]					0.71			
Eq. (20)		0.42						
Eq. (22)							0.73	
Eq. (25)	0.87	0.39	0.77	0.49	0.57	0.76	1.47	2.0

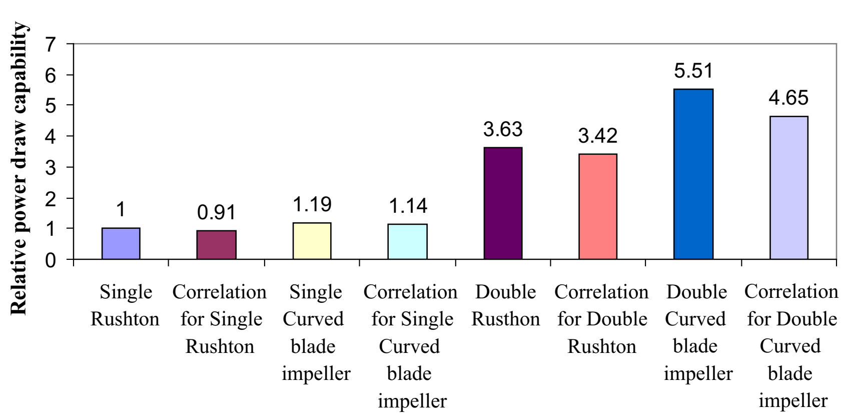

Fig. 4. Relative power draw capability with respect to the single Rushton with other configuration (case 2, 4, 7, 8).

Please cite this article in press as: T.T. Devi, B. Kumar, Mass transfer and power characteristics of stirred tank with Rushton and curved blade impeller, Eng. Sci. Tech., Int. J. (2016), http://dx.doi.org/10.1016/j.jestch.2016.11.005

the same amount of mass transfer capability to be achieved, the efficiency of a stirred tank can be understood from the power draw capability of the system. Hence, in this study also, there is no significant difference of mass transfer in Rushton and curved blade impeller predicted; however, there is great difference in power draw capability much higher by the curved blade than the Rushton impeller. The efficiency or energy efficiency is being shown in the Table 5, indicates that overall efficiency higher in the case of curved blade impeller (8.14% more efficient in single and 21.93% in double impeller) than the Rushton impeller.

5. Conclusion

Boundary condition plays important role to correctly predicting the fluid flow characteristics in stirred tank when more than one phase is involved. It is ascertained that degassing boundary condition predicts acceptably accurate results than the commonly used velocity-inlet condition. Among different mass transfer models, eddy cell model and slip velocity models predict the mass transfer coefficient in acceptable ranges. Higher power draw capability is predicted by curved blade than the Rushton impeller, which is 16% and 34% more in single and double impeller. Double impeller predicts higher power draw capability (70–80%) than the single impeller. In order to achieve the same mass transfer coefficient, curved blade impeller exhibits higher efficiency (8.14% more efficient in single and 21.93% in double impeller) than the Rushton impeller. Therefore, it has been concluded in this study that curved blade has more gas dispersion capability than the Rushton impeller even though both produces same amount of mass transfer rate.

References

[1] S.U. Ahmed, P. Ranganathan, A. Pandey, S. Sivaraman, Computational fluid dynamics modeling of gas dispersion in multi impeller bioreactor, J. Biosci. Bioeng. 109 (2010) 588–597.
[2] S.S. Alves, C.I. Mania, J.M.T. Vasconcelos, Experimental and modelling of gas dispersion in double turbine stirred tank, Chem. Eng. Sci. 89 (2002) 109–117.
[3] A. Bakker, 2000, A new gas dispersion impeller with vertically asymmetric blades, The Online CFM Book (available at http://www.bakker.org/cfm).
[4] W. Bujalski, A.W. Nienow, S. Chatwin, M. Cooke, Dependency on scale of power numbers of Rushton disc turbines, Chem. Eng. Sci. 42 (1987) 317–326.
[5] P.H. Calderbank, Physical rate processes in industrial fermentation: part 1 "The interfacial area in gas liquid contacting with mechanical agitation", Trans. Inst. Chem. Eng. 37 (1958) 443–463.
[6] P.V. Danckwerts, Significance of liquid-film coefficients in gas absorption, Indus Eng. Chem. 43 (1951) 1460–1467.
[7] T.T. Devi, B. Kumar, Scale up criteria for dual stirred gas-liquid unbaffled stirred tank with concave blade impeller, Korean J. Chem. Eng. 31 (2014) 1339–1348, http://dx.doi.org/10.1007/s11814-014-0090-7.
[8] S.E. Elgobashi, M.A. Rizk, A two-equation turbulence model for dispersed dilute confined two-phase flows, Int. J. Multiphase Flow 15 (1989) 119–133.
[9] M. Elqotbi, S.D. Vlaev, L. Montastruc, I. Nikov, CFD modelling of two-phase stirred bioreaction systems by segregated solution of the Euler-Euler model, Comput. Chem. Eng. 48 (2013) 113–120.
[10] N. Frossling, Uber die Verdunstung fallenden tropfen, Gerlands Beitage Geophys. 52 (1938) 170–216.
[11] K.M. Gezork, W. Bujalski, M. Cooke, A.W. Nienow, The transition from homogeneous to heterogeneous flow in a gassed stirred vessel, Chem. Eng. Res. Des. 78 (2000) 363–370, http://dx.doi.org/10.1205/026387600527482.
[12] J. Gimbun, C.D. Rielly, Z.K. Nagy, Modelling of mass transfer in gas-liquid stirred tanks agitated by Rushton turbine and CD-6 impeller: a scale-up study, Chem. Eng. Res. Des. 87 (2009) 437–451.
[13] R. Higbie, The rate of absorption of a pure gas into a still liquid during short periods of exposure, Trans AICHE 31 (1935) 364–389.
[14] H. Ameur, Agitation of yield stress fluids in different vessel shapes, Eng. Sci. Technol. Int. J. 19 (1) (2016) 189–196.
[15] G.A. Hugmark, Power requirements and interfacial area in gas-liquid turbine agitated systems, Indus Eng. Chem. 19 (1980) 638–641.
[16] A. Kapic, T.J. Heindel, Correlating gas-liquid mass transfer in a stirred tank reactor, Chem. Eng. Res. Des. 84 (2006) 239–245.
[17] F. Kerdouss, A. Bannari, P. Proulx, R. Bannari, M. Skrga, Y. Labrecque, Two-phase mass transfer coefficient prediction in stirred vessel with a CFD model, Comput. Chem. Eng. 32 (1943–1955) (2008) 010.
[18] A.R. Khopkar, J. Aubin, C. Xureb, N. Le Sauze, J. Bertrand, V.V. Ranade, Gas-liquid flow generated by a pitched blade turbine: PIV measurements and CFD simulations, Ind. Eng. Chem. Res. 42 (2003) 5318–5332.
[19] A.R. Khopkar, P.A. Tanguy, CFD simulation of gas-liquid flows in stirred vessel equipped with dual Rushton turbines: influence of parallel, merging and diverging flow configurations, Chem. Eng. Sci. 61 (2008) 3810–3820.
[20] S.S. Kshatriya, A.W. Patwardhan, A. Eaglesham, Experimental and CFD characterization of gas dispersing asymmetric parabolic blade impellers, Int. J. Chem. Reactor Eng. 5 (2007) 1–13.
[21] M. Laakkonen, P. Moilanen, V. Alopaeus, J. Aittamaa, Modelling local bubble size distributions in agitated vessels, Chem. Eng. Sci. 62 (2007) 721–740.
[22] J.C. Lamont, D.S. Scott, An eddy cell model of mass transfer into the surface of a turbulent liquid, AIChE J. 16 (1970) 513–519.
[23] M. Martin, F.J. Montes, M.A. Galan, Mass transfer rates from bubbles in stirred tanks operating with viscous fluids, Chem. Eng. Sci. 65 (3814) (2010) 3824.
[24] M. Martin, F.J. Montes, M.A. Galan, On the contribution of the scales of mixing to the oxygen transfer in stirred tanks, Chem. Eng. J. 145 (2008) 232–241.
[25] T. Moucha, V. Linek, K. Erokhin, J.F. Reji, M. Fujasova, Improved power and mass transfer correlations for design and scale-up of multi-impeller gas-liquid contactors, Chem. Eng. Sci. 64 (2009) 598–604.
[26] Y.L. Moullec, C. Gentric, O. Potier, J.P. Leclerc, CFD simulation of the hydrodynamics and reactions in an activated sludge channel reactor of wastewater treatment, Chem. Eng. Sci. 65 (2010) 492–498.
[27] K.J. Myers, A.J. Thomas, A. Bakker, M.F. Reeder, Performance of gas dispersion impeller with vertically asymmetric blades, Chem. Eng. Res. Des. 77 (1999) 728–730.
[28] T. Panda, Bioreactors Analysis and Design, Tata McGraw Hill, New Delhi, 2011.
[29] V.V. Ranade, Computational Flow Modeling for Chemical Reactor Engineering, Academic Press, A Harcourt Science and Technology Company, California, USA, 2002.
[30] P. Ranganathan, S. Sivaraman, Investigations on hydrodynamics and mass transfer in gas-liquid stirred reactor using computational fluid dynamics, Chem. Eng. Sci. 66 (2011) 3108–3124.
[31] J.M. Smith, Large multiphase reactors some open questions, Chem. Eng. Res. Des. 84 (2006) 265–271.
[32] M. Taghavi, R. Zadghaffari, J. Moghaddas, Y. Moghaddas, Experimental and CFD investigation of power consumption in a dual Rushton turbine stirred tank, Chem. Eng. Res. Des. 89 (2011) 280–290.
[33] K. Van't Riet, Review of measuring methods and nonviscous gas-liquid mass transfer in stirred vessels, Ind. Eng. Chem. Process Des. Dev. 18 (1979) 357–364.
[34] D. Wadnerkar, R.P. Utikar, M.O. Tade, V.K. Pareek, CFD simulation of solid-liquid stirred tanks, Adv. Power Technol. 23 (2012) 445–453.
[35] M.M.C.G. Warmoeskerken, J.M. Smith, 1982, Description of the power curves of turbine stirred gas dispersions, in: Proceedings of the Fourth European Conference on Mixing Noordwijkerhout, BHRA, Granfield.
[36] M.H. Xie, J.Y. Xia, G.Z. Zhou, S.L. Zhang, P.Q. Yu, Hydrodynamics characterization of an ellipse gate impeller by experimental and numerical studies, Chem. Eng. Technol. 36 (2013) 115–122.
[37] R. Zadghaffari, J.S. Moghaddas, J. Revstedt, Large eddy simulation of turbulent flow in a stirred tank driven by a Rushton turbine, Comput. Fluids 39 (2010) 1183–1190.
[38] D. Zhang, N.G. Deen, J.A.M. Kuipers, Numerical simulation of the dynamic flow behavior in a bubble column: a study of closures for turulence and interface forces, Chem. Eng. Sci. 61 (2006) 7593–7608.
[39] Y. Zhu, P.C. Bandopadhayay, J. Wu, Measurement of gas–liquid mass transfer in an agitated vessel-A comparison between different impellers, J. Chem. Eng. Jpn. 34 (2001) 579–584.

Please cite this article in press as: T.T. Devi, B. Kumar, Mass transfer and power characteristics of stirred tank with Rushton and curved blade impeller, Eng. Sci. Tech., Int. J. (2016), http://dx.doi.org/10.1016/j.jestch.2016.11.005